Cluster evolution in steady-state two-phase flow in porous media

Thomas Ramstad* and Alex Hansen†
Department of Physics, Norwegian University of Science and Technology, N-7491 Trondheim, Norway
(Received 11 November 2005; published 13 February 2006)

We report numerical studies of the cluster development of two-phase flow in a steady-state environment of porous media. This is done by including biperiodic boundary conditions in a two-dimensional flow simulator. Initial transients of wetting and nonwetting phases that evolve before steady state has occurred, undergo a crossover where every initial pattern is broken up. For flow dominated by capillary effects with capillary numbers in order of 10^{-5}, we find that around a critical saturation of nonwetting fluid the nonwetting clusters of size s have a power-law distribution $n_s \sim s^{-\tau}$ with the exponent $\tau = 1.92 \pm 0.04$ for large clusters. This is a lower value than the result for ordinary percolation. We also present scaling relation and time evolution of the structure and global pressure.

DOI: 10.1103/PhysRevE.73.026306 PACS number(s): 47.56.+r, 05.40.−a, 07.05.Tp, 47.54.−r

I. INTRODUCTION

The complex nature of multiphase flow in porous media has acted as motivation for extensive studies in the recent years. Different types of fluid displacements in porous media play important roles in natural processes, many of them of large practical importance such as oil recovery, soil mechanics, and hydrology. Large quantities of petroleum and water resources are hidden in fractured and porous stones and that is of vast economic and social importance.

Two-phase displacement in porous media has been studied through seminal experimental work [1–3], numerical simulations [4–6], and theoretical work including statistical models and differential equations [7,8]. Dynamics of instabilities in immiscible two-phase flow controlled by the interplay between viscous and capillary forces give rise to complex pattern formations.

The traditional way of describing those situations has been through either drainage or imbibition. That will give rise to transient effects of front propagation such as invasion percolation (IP), viscous fingering, and stable front displacement. The common feature of these effects is that they are out of equilibrium, and the IP regime will eventually even end with a static regime with immobile structures due to large capillary barriers. Most experiments and simulations in this area deal with systems where one and only one fluid is injected into another until the injected fluid reaches the sink of the system. In natural reservoirs of fluid in porous media the situation is, however, dynamic and governed by the interplay and competition between drainage and imbibition. This is best described as a steady-state regime inside a representative volume element where both drainage and imbibition occurs. Pure drainage or pure imbibition are pore-scale concepts, and can therefore not alone be scaled up in a steady-state situation.

In this paper we examine distribution of cluster formations in a pore-scale network under both steady state and transients. This study contains both quantitative and qualitative results of cluster distribution and dynamic evolution of the phases. The model used in our simulations is mainly similar to that proposed by Aker *et al.* [9] with later generalizations by Knudsen *et al.* [10] to include *biperiodic* boundary conditions. The boundary conditions in the flow direction lets the fluid that leaves the system enter the system again at the inlet of the model in a seamless manner.

This enables us to investigate steady-state flow which inflects the situation deep inside reservoirs. With both an invading front of nonwetting fluid and wetting imbibition the system will give rise to a blending of structure formations. These formations are formed by the interplay of different effects like fragmentation of large clusters, merging of smaller clusters, and a diffusion of fragments.

This paper is organized in the following way. In Sec. II we describe outlines of the model used for our simulations, and in Sec. III we sketch the initial conditions used followed by a discussion of the qualitative behavior of initial transients.

Further, we discuss quantitative features of the simulations in Sec. IV, prior to a scaling analysis.

II. MODEL

The main statistical models that reproduce the basic domains of porous flow belong to the family of growth models that obey the Laplacian equation $\nabla^2 P = 0$ where P is a pressure field and with an interfacial growth rate $q \propto \nabla P$.

The simulations used in this work are based upon a basis model of disordered media that consists of tubes orientated 45 degrees to the overall flow direction [9,10]. The network has a coordination number of 4, and the arrangement of the tubes is square planar. The tubes consist of both the pore volume and the throat volume. The points where the tubes meet are referred to as nodes. Randomness is incorporated in the model by allowing the length of the tubes d_{ij} to be chosen randomly within 30% of the mean length, i.e., the lattice constant d, and the radii to be chosen from a flat distribution $r \in (0.1d, 0.1d + 0.3d_{ij})$.

*Electronic address: Thomas.Ramstad@phys.ntnu.no
†Electronic address: Alex.Hansen@ntnu.no

Distributions of fluid that we report are highly dependent on saturation of phases and the capillary number (Ca), where

$$Ca = \frac{\mu Q_{tot}}{\gamma \Sigma} \tag{1}$$

denotes the ratio between viscous and capillary forces, and μ is the largest viscosity rate of the two fluids, γ is the surface tension, Σ denotes the total input surface of the system, and Q_{tot} is the global flow rate in the system. The patterns that form during invasion of a nonwetting fluid into a defending wetting one are characterized mainly into viscous fingering, capillary fingering, or stable displacement depending on Ca and the viscosity ratio of the defending μ_1 and invading phase μ_2 given by

$$M = \frac{\mu_{\mathrm{nw}}}{\mu_{\mathrm{w}}}. \tag{2}$$

Our system of tubes is filled with two fluids, wetting and nonwetting, respectively, each having a certain fraction of the total volume, denoting nonwetting saturation S_{nw} and wetting saturation S_{w}. The fluids are separated through many menisci. The model does not include film flow and only one bubble is allowed inside one tube at the time. This means that if more than two menisci are created within a tube during the same time step, they are subsequently collapsed into two menisci.

Since the fluids are immiscible, the meniscus gives rise to a capillary pressure within the tube. The capillary pressure is dependent on both the surface tension γ and the radius of the tube given by the Young-Laplace law

$$p_c = \frac{2\gamma}{r} \cos\theta, \tag{3}$$

where θ is the wetting angle, i.e., the contact angle between the wetting phase and the wall of the tube. In our model, the tubes are considered to be cylindrical with respect to permeability, but hourglass shaped with respect to capillary pressure. The relation for the capillary pressure reads

$$p_c = \frac{2\gamma}{r}[1 - \cos(2\pi x)], \tag{4}$$

where x is the normalized position of the meniscus running from 0 to 1. The local flow rate q of a tube follows the Washburn equation for capillary flow [11],

$$q = -\frac{k}{\mu_{\mathrm{eff}}} \frac{\pi r^2}{d} (\Delta p - p_c), \tag{5}$$

where p_c is given by Eq. (4) and the permeability $k = r^2/8$. This permeability is taken directly from Hagen-Poiseulle flow in cylindrical tubes. We define the effective viscosity as

$$\mu_{\mathrm{eff}} = \mu_{\mathrm{nw}} x_{\mathrm{nw}} + \mu_{\mathrm{w}}(1 - x_{\mathrm{nw}}), \tag{6}$$

with respect to the position of the nonwetting meniscus x_{nw}. The pressure difference between the inlet and outlet of a tube is Δp.

To solve the transport equations we use the property that no net volume can be stored in the nodes connecting tubes. The net flux through a node is therefore zero and this gives a set of linear equations to solve. To find the positions of menisci in the tubes we integrate Eq. (5) forward with a predefined time step, Δt, according to an explicit Euler scheme. Inside a tube one meniscus moves with a front speed determined from the local flow rate q, but when a meniscus reaches the end of a tube it is further distributed among the other tubes with ingoing flux. Here it is crucial that volume is conserved. Further details can be found in Refs. [9,10].

The majority of existing models are quasistatic and therefore apply only when the capillary forces are dominant. This model, however, accounts for dynamic effects and is therefore also capable of handling fast flow or flow with little surface tension, hence a wider range of the capillary number Ca.

Boundary conditions

Boundary conditions. Most experimental setups and simulations are done on systems that are out of steady state. They mainly deal with systems where one fluid is injected into another defending fluid and ends when the invading fluid has reached the sink of the model.

In order to simulate steady-state flow, we use *biperiodic boundary conditions*. This is done by connecting the inlet and outlet row, placing the system on a surface with one extra dimension. In two dimensions this is easily pictured by placing it on a three-dimensional torus as shown in Fig. 1.

To make the system develop in time, the global pressure field ΔP is applied over the row where the original inlet and outlet rows meet. This is done by the use of *ghost sites* [12] where the global pressure is applied.

With biperiodicity in the boundary conditions we will have two invading processes that compete. One is the original invading process as described above with a nonwetting phase penetrating a wetting phase, but there will also be a wetting phase displacing a nonwetting phase since the wetting fluid imbibition from the system will enter it at the inlet row.

III. INITIAL TRANSIENTS

In this section we describe the qualitative behavior of our system as it evolves. As time progresses, the dynamic evolution in our model will give rise to different transient effects that eventually will lead to a steady-state configuration. These transients are dependent on the control parameters in our system.

Typical parameters that are fixed during our simulations are surface tension γ and viscosity μ. We keep $\gamma = 30$ mN/m and $\mu_{\mathrm{nw}} = \mu_{\mathrm{w}} = 0.1$ Pa s which gives the viscosity ratio $M = 1$. In order to set the capillary number, we control the overall flow rate Q_{tot}.

In this paper we consider networks of sizes up to 1024×1024 nodes. We wish to analyze the distributions of clusters with different Ca and different system sizes.

At the beginning of the simulations, the network is segregated into one part of nonwetting fluid and one part containing only wetting fluid. At the start of the simulation the non-

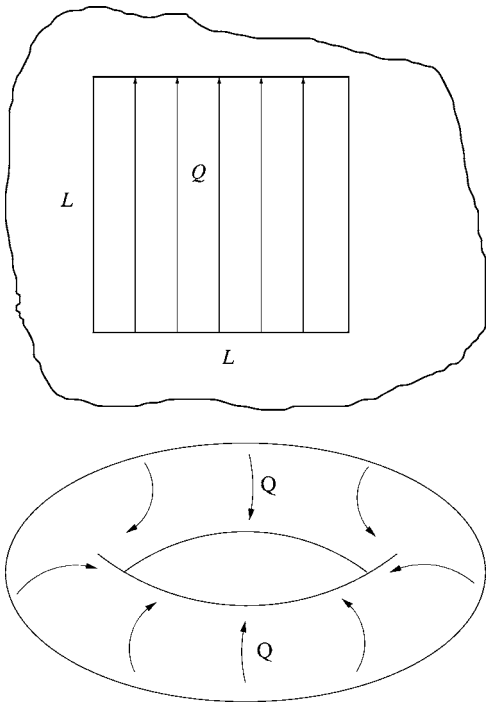

FIG. 1. Schematic figure that shows the interpretation the *biperiodic boundary conditions* mean to our simulations. In order to model a situation deep inside a natural reservoir in steady state, we must consider the system size as a small part of a greater system. Statistically, it is the same fluid configurations entering the element as are leaving it. This is illustrated in the upper figure. The way we consider our system is shown on the lower figure where the two-dimensional system is mapped onto a three-dimensional torus.

wetting fluid will start to invade the wetting fluid part. Depending on the capillary number it will either start a viscous fingering behavior for high *Ca* or an IP process when the capillary forces dominate. The latter case is visualized in Fig. 2 where the drainage takes place in the upper part of the system. In the early stages presented in the figure, a "belt" of nonwetting (black) fluid spans the system in horizontal direction. This "belt" is an initial configuration chosen by us and will be referred to later in this paper.

On the other hand, wetting fluid will enter the original nonwetting region from below, pushing the nonwetting fluid in the advancing direction. This displacement of nonwetting fluid in favor of the wetting happens in a pistonlike manner. There are some trapped regions left of nonwetting fluid, but these are smaller than the trapped wetting clusters in the other end of the model. Since the nonwetting front fingers advance more rapidly than the wetting, more compact propagating front [29], it will sooner or later catch up with the front of the advancing wetting fluid. At this point there will be a competition between the two different advancing fronts.

When the system reaches steady state there will be a mixing of the two phases. This mixing is dependent on both *Ca* and the saturation of fluids. If the difference in the saturation of fluids is large, one of the phases will span the system entirely, in steady state, with a large cluster. How large this difference needs to be in order to get a spanning cluster depends on the capillary forces and the structure of the network, i.e., the porosity. If the capillary forces dominate over the viscous ones, the single phase pressure P_s, according to Darcy's law,

$$\frac{Q}{\Sigma} = \frac{k}{\mu}\frac{\Delta P_s}{L}, \tag{7}$$

where L is the system length along the single phase gradient ΔP_s, will be significantly smaller than the total pressure gradient. In this case if there is a spanning cluster of one fluid it will be much easier for the fluid to move inside this cluster because of the high capillary pressure threshold in unoccupied tubes. As a consequence once a spanning cluster evolves, the total pressure will drop and one phase stays immobile or trapped.

Since the total flux is constant and the capillary pressure will vary with time as menisci configurations change, the global pressure will fluctuate. However, when the system reaches steady state, the pressure will fluctuate around a mean value. How long it takes before our system reaches steady state is a matter of the initial configuration of the two fluids. As the pressure relaxes around a mean value the fractional flow of each fluid will settle. The nonwetting fractional flow is defined as $F_{\mathrm{nw}}=Q_{\mathrm{nw}}/Q_{\mathrm{tot}}$ and the wetting fractional flow is $F_{\mathrm{w}}=Q_{\mathrm{w}}/Q_{\mathrm{tot}}$.

It has been shown in previous work [10,13] that F_{nw} depends on both the capillary number and the saturation S_{nw} of the nonwetting fluid. For high values of *Ca*, the curve of F_{nw} will behave almost linearly with respect to S_{nw}, while in the case of very small *Ca* we will get regimes where one fluid is almost immobile. This feature was also found to be independent of system size.

For steady-state flow we are only able to obtain a totally immobile regime or a dynamic regime where clusters rearrange themselves continuously. The first situation can be characterized as traditional invasion percolation where capillary forces dominate. When a percolating cluster arises, the structure stays static as long as no global parameters are changed. There will be a sudden drop in global pressure P as no capillary barriers will have to be overcome to sustain the global flow rate.

In the opposite case, clusters of fluid move, fragment, and coalesce in an equilibrium process with a global pressure fluctuating around a mean value. This is true for the viscous case where clusters are not trapped inside a growing percolating cluster. However, we report in this paper that this is also the case in a steady-state situation even for very low *Ca* which should indicate that capillary forces dominate.

If, on the other hand, *Ca* is large and viscous forces dominate, we will need a much larger difference in S to get a spanning cluster. This is because trapping of fluid is less likely to happen and therefore large clusters are more vulnerable to fragmentation through creation of bubbles. In the extreme case, where there are no capillary forces at all, a homogeneous mixing will occur.

Pressure development

For small *Ca* and subsequently large influence of capillary forces, the pressure buildup is initially slow. A regular struc-

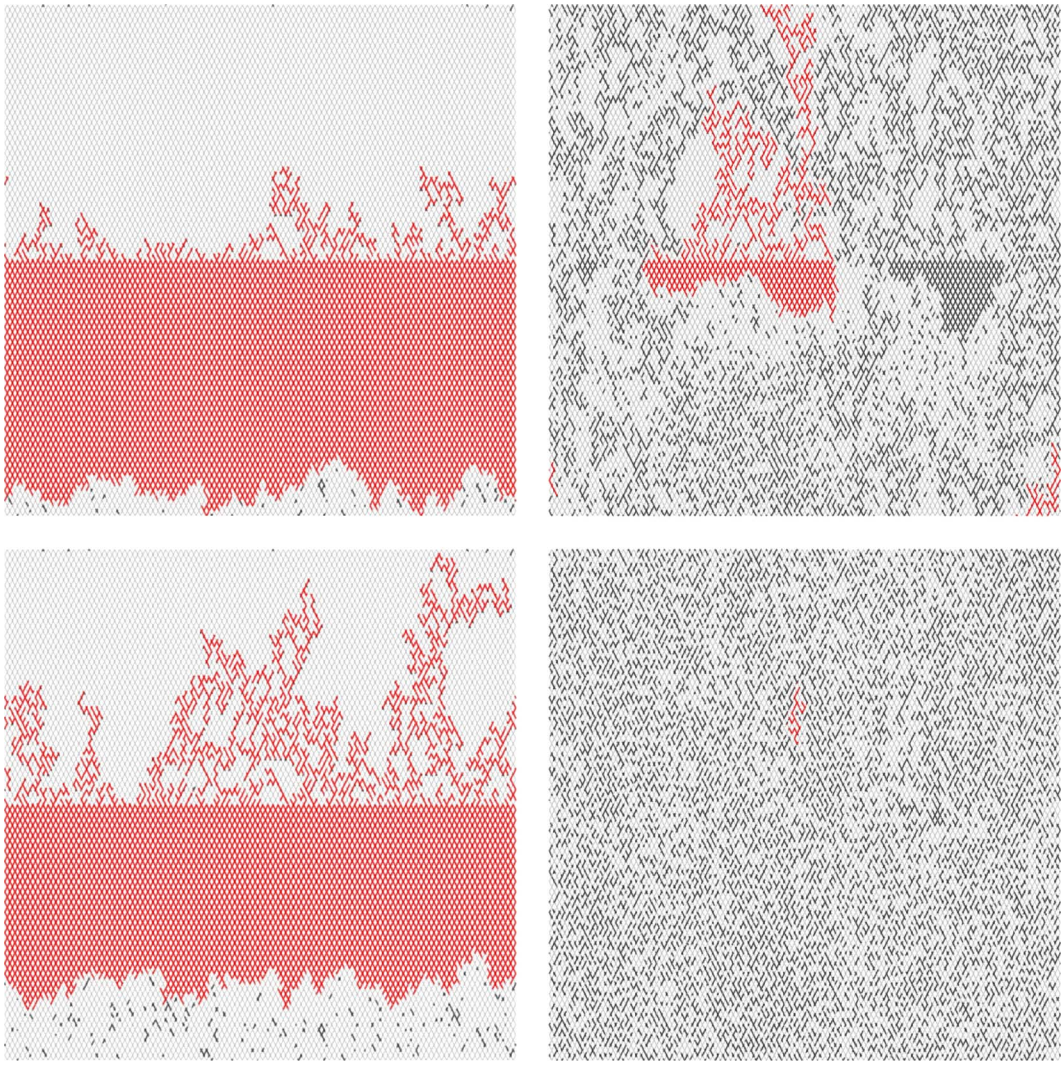

FIG. 2. (Color online) Four different stages of a low Ca flow configuration with viscosity match $M=1$ $Ca=3.2\times10^{-5}$ implies a capillary-dominant regime. The different snapshots of the flow patterns are taken at $t=5000$ s, $t=10\,000$ s, $t=15\,000$ s, and $t=25\,000$ s. The system size is 128×128 with a $S_{\mathrm{nw}}=0.5$. The largest connected cluster is colored red in the online version of the article. The two first snapshots correspond to the first regime of the pressure in Fig. 3. In the third snapshot some of the initial configuration is still left and the pressure is building up according to Fig. 3. The last one is in the steady state regime where every initial structure has vanished.

ture of the fluid clusters will decrease the global pressure since the capillary part of the global pressure is dependent on the overall structure and the single-phase pressure $P_s \ll P_c$.

For low capillary numbers the nonwetting fluid will be blocked in the area around the nodes due to the capillary barriers of the tubes. Wetting fluid will therefore in large parts of the system be immobilized. This trapping of fluid gives a lower fractal dimension $\tilde{D}$ of the invading IP structure.

For low Ca, the drainage of the IP part will eventually meet the compact imbibition front of the wetting fluid due to *biperiodic boundary conditions*. As long as the source of the drainage transient has an intact "belt," as shown in Fig. 2, in the direction normal to the flow direction, the invading front will move through bursts in the local pressure. These have a well-defined distribution [14]. This regime is seen in Fig. 3 early in the pressure evolution as a region with a slowly increasing mean pressure.

When the first nonwetting fingers start to coalesce with the stable displacement of the wetting fluid after having completed a turn along the torus, a competition between two different processes arises. If the percolating nonwetting cluster is not sustained and subsequently broken, P_c will increase.

Eventually the initial IP cluster will break up and fragment into smaller clusters as shown in the third picture of Fig. 2. When there is no initial structure left in the system, the pressure saturates around a mean value with larger fluctuations than the previous case with the small bursts.

The pressure development in Fig. 3 can be divided in three different segments. For this case where the injection rate is slow, the first segment describes an IP regime where the P_c only describes local capillary fluctuations for the menisci movement along the front. The trapped clusters of wetting fluid will have little effect on the effective viscosity of the nonwetting fluid and the front is not saturated.

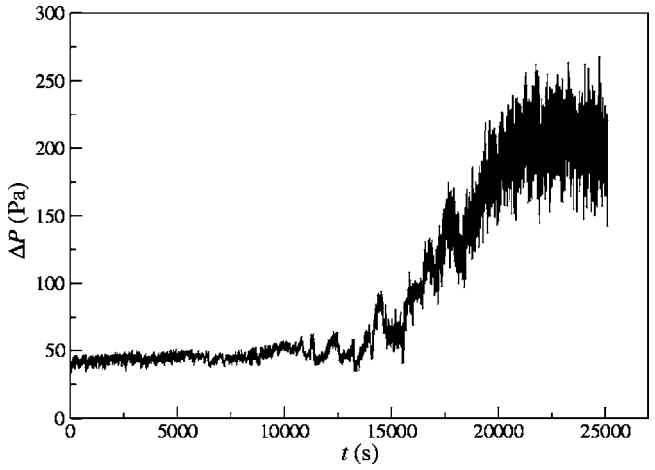

FIG. 3. Dynamic evolution of global pressure in a 128×128 system at $Ca=3.2\times10^{-5}$ and $M=1$. In the initial phase of the flow evolution there is a small buildup in pressure, but when the wetting front breaks through the initial belt of nonwetting fluid the increase in pressure is violent. At the last, steady state, regime the fluctuations are approximately five times larger than in the first regime.

In the second segment we see a drastic increase in ΔP. Since the system is having the same injection rate and therefore is governed by capillary effects, this means that the effective dynamic viscosity μ_{nw} has increased and the viscosity ratio $M>1$. A qualitative explanation for this increase in viscosity can be seen in connection to the reduced permeability of the invaded, wetting region caused by trapped nonwetting clusters left behind by the compact wetting front. The nonwetting front has reached saturation width w_s. The result is a more stable front, and it was pointed out by Aker *et al.* [15] that P_c is proportional to the height difference in the front

$$P_c \propto \Delta h^{\kappa}, \tag{8}$$

where $\kappa=1$.

In the third and last segment, the flow has reached steady state. The fluctuations in P_c are larger and the mean value higher due to the unstructured pattern of fluids.

IV. STEADY-STATE DISTRIBUTIONS

In this section we look particularly at the distribution of nonwetting clusters. Because of the capillary barriers the nonwetting fluid has a much higher tendency to occupy pore volume near the nodes rather than around the throats in the network. Due to volume conservation of wetting fluid, this will block the throats and create loopless fingers of nonwetting fluid. Movement of trapped clusters must occur, and the steady-state fragmentation and merging of nonwetting clusters $N(s,t)$ is

$$\partial_t N(s,t) = [\partial_t N]_{\mathrm{merging}} + [\partial_t N]_{\mathrm{frag}} = 0. \tag{9}$$

A. Distribution of clusters

The distribution of clusters depends on size. Fragmentation and merging of clusters in various dimensions are described, e.g., in Refs. [16–18].

At steady state there will be a typical size s^* of the clusters, and clusters of size $s\gg s^*$ are very rare. The distribution of clusters $N(s,L)$ consists of both a regular and a singular part, $N(s,L)=N_{\mathrm{reg}}(s,L)+N_{\mathrm{sing}}(s,L)$, and for saturations S_{nw} close to or equal to a critical saturation S_c, the singular part of $N(s,L)$ will dominate.

Based on analogy to percolation and finite-size scaling [25], we assume the general expression for the singular distribution to be

$$N_{\mathrm{sing}}(s,L) \propto L^{\chi} s^{-\tau} f\left(\frac{s}{s^*}\right), \tag{10}$$

where $f(x)$ is a cutoff function decaying faster than any power law for $x\gg1$ and is constant for $x\ll1$. The exponent χ which governs the system size dependence of N_{sing}, has the value $\chi=d$ in pure percolation. We have it here undetermined.

When the clusters have a fractal dimension D, the typical size $s^*\propto l^D$, where $l=\min(L,\xi)$, where ξ is the correlation length. For large system sizes, the area A the clusters occupy is

$$A = \int^{\infty} sN(s,L)ds = \int^{\infty} s(N_{\mathrm{reg}}+N_{\mathrm{sing}})ds = A_{\mathrm{reg}} + A_{\mathrm{sing}}, \tag{11}$$

and the singular part scales as

$$A_{\mathrm{sing}} \sim L^{\chi}\int^{\infty} s^{1-\tau} f\left(\frac{s}{s^*}\right)ds = L^{\chi}(s^*)^{2-\tau}\int^{\infty} x^{1-\tau}f(x)dx. \tag{12}$$

The lower limit of Eq. (12) converges when we exclude arbitrary small clusters, and as a result

$$A_{\mathrm{sing}} \sim L^{\chi}(s^*)^{2-\tau} = L^{\chi+(2-\tau)D}, \tag{13}$$

when we use that $s^*\propto L^D$ near critical saturation.

Long before steady state, the nonwetting fluid forms IP patterns, and the total area $A\propto s^*$. The saturation of the invading, nonwetting fluid, then depends on the fractal dimension D and will scale locally as [19]

$$S_{\mathrm{nw}} \propto L_{loc}^{D-d}, \tag{14}$$

where L_{loc} is limited to the region where the defending fluid is purely wetting. Due to the incompressibility of the two phases, trapped fluids around the hull of the spanning, invading cluster causes the saturation of invading fluid to decrease even more as the system size L is increased.

We have that $A=A_{\mathrm{sing}}$ locally because this is in the pure IP regime, and there are no fragments of nonwetting fluid. Following Meakin [20], the scaling of the singular cluster surface is

$$A_{\mathrm{sing}} = \int^{\infty} sN_{\mathrm{sing}}(s,L)ds \sim L^d\int^{\infty} s^{1-\tau} f\left(\frac{s}{s^*}\right)ds, \tag{15}$$

which gives $A_{\mathrm{sing}}\sim L^{d+(2-\tau)D}\sim L^D$ and

$$\tau = \frac{D+d}{D}. \tag{16}$$

In percolation, the fractal dimension of a spanning cluster is $D(p=p_c)=91/48$ giving $\tau \approx 2.05$. In the regime where we have invasion percolation the area of wetting defending clusters behaves as

$$A = \int^{\infty} sN(s)ds \sim L^D \int^{\infty} s^{1-\tau} f\left(\frac{s}{s^*}\right) ds. \tag{17}$$

It was found that for IP structure, A grows as L^d, which imposed a $\tau < 2$ and $A \sim L^{D+(2-\tau)d} \sim L^d$. This gives $\tau = 1 + D/d$ and with a fractal dimension $D=1.82$ with trapped wetting clusters, this gives $\tau = 1.91$ for the distribution of wetting clusters.

When steady state is reached the mean saturation of the two phases stays constant over the entire system and every pattern created by the transients is wiped out. We write the nonwetting saturation as

$$S_{\mathrm{nw}} = \int^{\infty} sn_s ds, \tag{18}$$

where $n_s = L^{-d} N(s,L)$. According to Eq. (11) we then get contributions to S_{nw} both from a regular and singular part of n_s. Since S_{nw} is constant and the spanning IP cluster is broken up, the probability that a given area fraction of nonwetting fluid is attached to the spanning cluster changes from unity to

$$P_{\infty} \propto (S_{\mathrm{nw}} - S_c)^{\beta} \sim L^{-\beta/\nu} \quad \text{for } S_{\mathrm{nw}} \geqslant S_c. \tag{19}$$

We take finite-size scaling into account and the correlation length $\xi \propto |S - S_c|^{-\nu}$ when S_{nw} is chosen not to be far from S_c.

The singular contribution to P_{∞} then gives the following relation between critical exponents

$$\frac{\beta}{\nu} = (\tau - 2)D + d - \chi \geqslant 0, \tag{20}$$

since $\beta \geqslant 0$ and $\nu \geqslant 0$, which gives

$$\tau \geqslant 2 - \frac{\chi - d}{D}. \tag{21}$$

From this, we can have a value of $\tau < 2$, if the exponent $\chi < d$. In percolation where $\chi = 2$ we must have a $\tau > 2$ in order to ensure a positive $\beta > 0$.

When we look at the probability n_s of having a cluster of size s in the limit of $L \to \infty$ it must approach an asymptotic, constant value. Since $n_{s,\mathrm{sing}} \leqslant n_s$ and

$$n_{s,\mathrm{sing}} \sim L^{\chi - d} s^{-\tau} f\left(\frac{s}{s^*}\right) \to \text{const} \times L^{\chi - d}, \tag{22}$$

as $L \to \infty$, and hence $s^* \to \infty$, this means that $\chi \leqslant 2$ for finite s. It is clear that our situation differs from ordinary percolation.

B. Evolution of wetting clusters

It has been shown both experimentally and in numerical studies that the width of an invading nonwetting front w_{nw} depends both on Ca and the time t of the evolution. The front width w of the invading front is calculated as the standard deviation of number of points $n(y)$ belonging to the front at a distance y from the average position of the same front. It has been proposed that w_{nw} scales width time as

$$w = t^{\beta_d} h(t, Ca), \tag{23}$$

where $h(t,Ca)$ is a crossover function. When the width of the front has reached saturation, i.e., at large time scales $t \gg w^{1/\beta_d}$, the saturation width w_{s} is no longer dependent on time and w_{s} is purely a function of Ca [21].

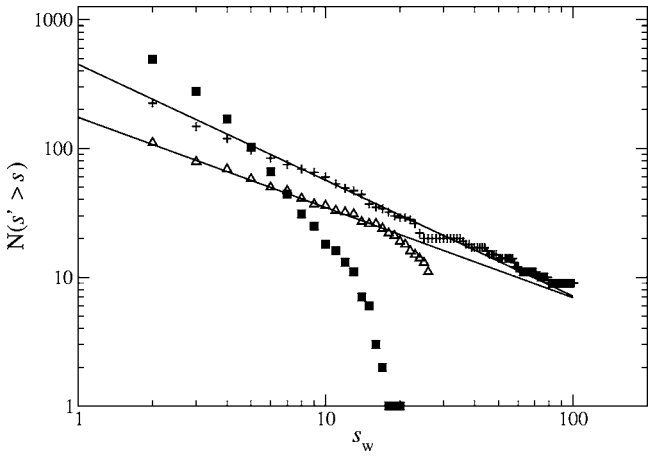

FIG. 4. Distribution of wetting clusters near the nonwetting front at different stages of evolution. The earliest stage (△) has a slope of 1.71. The cutoff here is due to lack of larger clusters that will evolve at later stages. As time increases (+), the slope is now 1.91, while at steady state (■) the power-law distribution is completely overrun by the cutoff function.

At low Ca, the front is wide and trapped clusters of wetting fluid exist on many different length scales. This situation is best described as IP with trapping, with a fractal dimension $D=1.82$ [22]. The distribution of these wetting clusters is shown in Fig. 4. We see a significant difference in the scaling at different times. The smallest exponent τ according to Eq. (10) is $\tau \approx 1.7$ which is consistent with the experimental findings by Frette *et al.* [21]. At this point there is a cutoff for large clusters as these have not yet had the time to form. In the latter case $\tau \approx 1.9$ which is in more correspondence with the scaling proposed by Meakin [20] in Eq. (17). When the system is in steady state, the wetting clusters are no longer trapped and the largest wetting clusters will break apart.

As Ca increases, the nonwetting front approaches a qualitatively more compact displacement [23,24]. Looped fingers will also occur since the capillary barrier is weak and there are no large, immobile wetting clusters as shown in Fig. 5.

C. Effect of saturation

For a certain saturation level S_{nw} of nonwetting fluid, at the equilibrium described in Eq. (9) the nonwetting fluid will percolate the system. We assume as in percolation theory [25] the singular distribution of clusters to be

$$N_{\mathrm{sing}}(s) \sim s^{-\tau} \exp\left(-\frac{s}{s^*}\right). \tag{24}$$

Since $s^* \propto \xi^D \propto |S_{\mathrm{nw}} - S_c|^{-\nu D}$, we can write the typical cluster size in means of saturation and get $s^* \propto |S_{\mathrm{nw}} - S_c|^{-1/\sigma}$. The

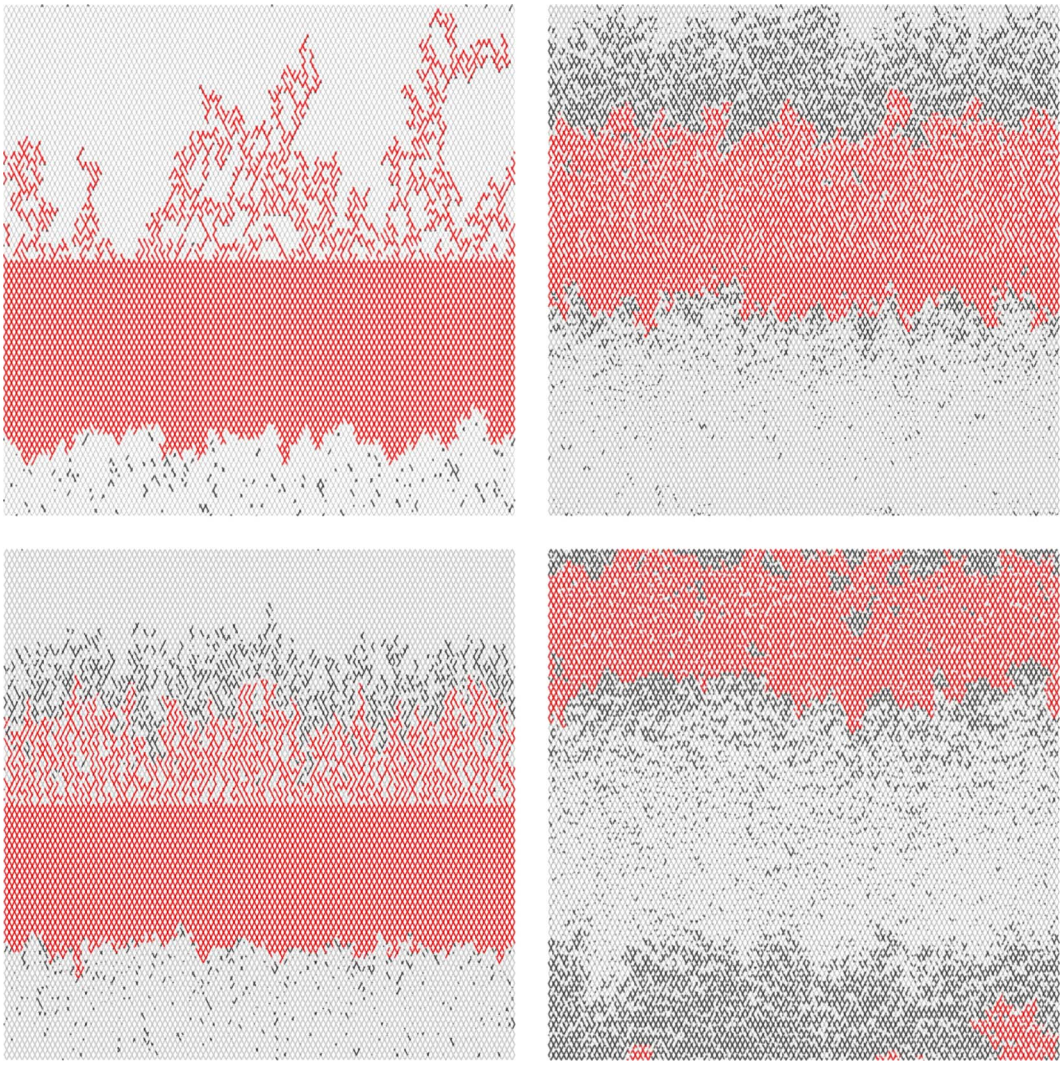

FIG. 5. (Color online) Four different snapshots of configurations with different Ca taken at approximately the same time. In the upper left figure $Ca=3.2\times10^{-5}$. For the next three figures Ca is much higher, $Ca=1,10$, and 100. The largest connected cluster is colored red in the online version of the article. The nonwetting front is now compact with high degree of fragmentation. The viscosity ratio of the two fluids is $M=1$, but the effective viscosity may be altered due to decreased permeability caused by fragmentation of the clusters.

exponent $\sigma=1/(\nu D)$, and for simplicity we define $c\propto|S-S_c|^{1/\sigma}$.

We have performed numerical tests of the above presumption with a matching viscosity ratio $M=1$. The tests have been initiated with both a complete separation of wetting and nonwetting fluids and a random mixing of the two phases. The question is whether or not the initial conditions will affect the steady-state outcome.

If there exists a fluid configuration that stems from the combined process of drainage and imbibition, the outcome of the two initial configurations described above should have the same statistical properties. However, for low Ca we encounter difficulties connected to "locking" of immobile configurations due to large capillary barriers. The time steps in our model become unphysically large. In order to compensate for these effects we apply certain shocks to the system where the input flow rate is increased drastically for a small amount of time steps compared to the total number of run time steps.

We now consider distributions of clusters obtained from different system sizes and initial configurations. The clusters are identified through a customized Hoshen-Kopelman algorithm [26]. The mass s of the clusters is a continuous variable, and in order to make a histogram we bin the identifed clusters with a bin size $\Delta s=s_{\max}\times1/10\,000$. The largest cluster $s_{\max}$ is five orders of magnitude larger than the unit size $s=1$.

As described in previous sections, the case where the two phases are completely separated gives intermediate configurations with different cluster distributions. The distributions depend on whether the fluid is invading or withdrawing from a region. In a study by Wagner *et al.* [27] experiments and simulations of fragmentation of nonwetting fluid were carried out. The case here was to take a full IP pattern, and reverse the fluid current so that the flow regime was changed from drainage to imbibition. A result to note in Ref. [27], is that when the nonwetting saturation of the IP pattern at breakthrough follows the relation in Eq. (14) as expected, the

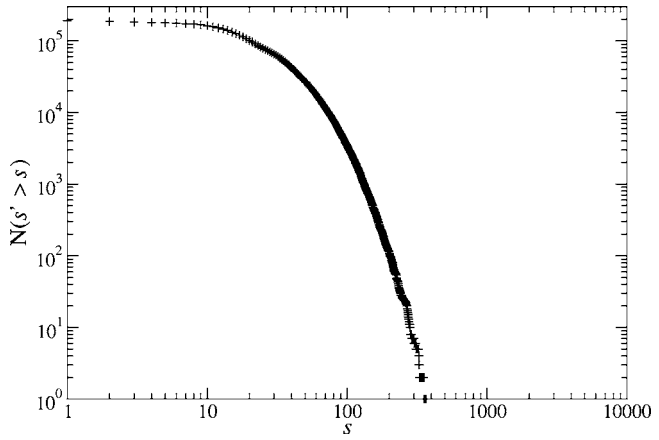

FIG. 6. Cumulative distribution $N(s' > s)$ of nonwetting clusters at steady-state flow regime for 128×512 system at $Ca = 3.2 \times 10^{-5}$. The results are from a simulation with $S_{nw} = 0.5$ and the clear cutoff at high s indicates that the critical saturation $S_c > 0.5$.

final saturation of nonwetting fluid seemed to be independent of system size.

In traditional simulation and experiments of imbibition and drainage of different fluids, there is a inlet flow of one phase into an already fully saturated region of another phase. In our simulations, the effective saturation of the two phases are constant throughout the entire experiments.

The percolation threshold for bond percolation in a regular square lattice is $p_c = \frac{1}{2}$. The distribution of clusters in the system referred to in Fig. 2 with $S_{nw} = 0.5$ has a clear cutoff for large cluster sizes s. It is therefore clear that—in order to see clusters of nonwetting fluid with size in order of the system size—we must have a larger saturation S_{nw} and $S_c > 0.5$, as shown in Fig. 6.

With a nonwetting saturation $S_{nw} = 0.69$ we see a tendency towards a power-law distribution of cluster size s. A closer study at the results in Fig. 7 reveals a value of the exponent $\tau - 1 = 0.91 \pm 0.03$ from the cumulative distribution $N(s' > s)$ while a value of $\tau = 1.93 \pm 0.05$ slightly lower than 2 is drawn from the ordinary distribution of $N(s)$. This is not very far from the prediction of ordinary percolation and consistent with predictions concerning similar dynamic models [28] which indicate a τ significantly smaller than 2.

It is hard to pinpoint the exact value of S_c in a system, but analysis of the cluster moments behavior gives us clear indications of the whereabouts of S_c.

D. Scaling analysis

In order to study scaling behavior in the fragmentation and merging process of Eq. (9), we examine different moments of cluster distribution.

The kth moment is defined as

$$M_k = \int^{\infty} s^k n_s ds, \tag{25}$$

and $n_s = n_{s,\mathrm{reg}} + n_{s,\mathrm{sing}}$, the moments will consist of both a regular and a singular part. We use percolation methods [25]

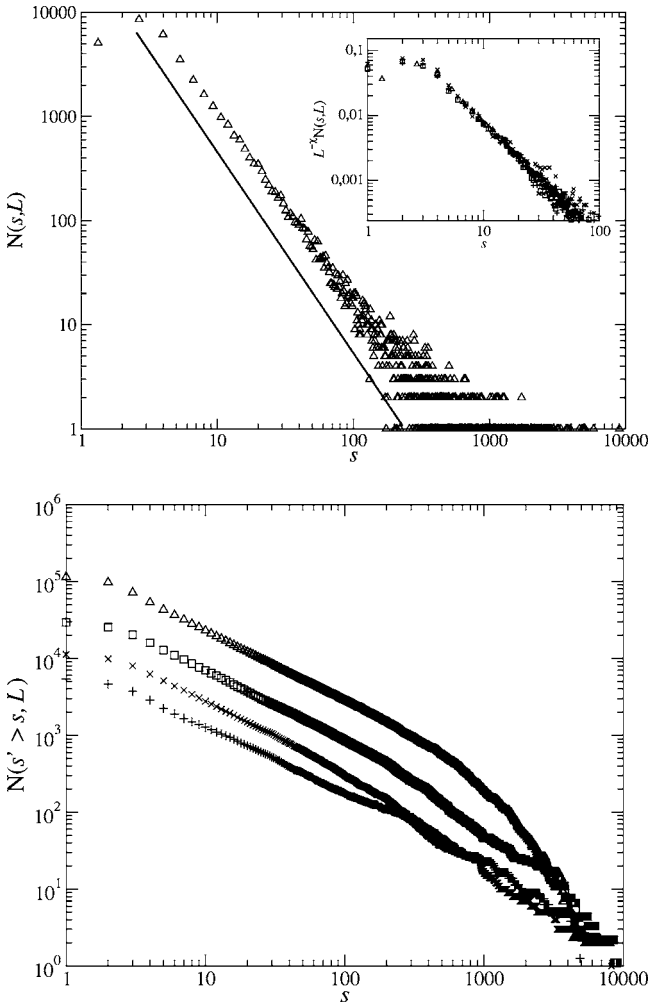

FIG. 7. Log-log plot of distribution of nonwetting clusters at $S_{nw} = 0.69$. The upper figure shows the distribution $N(s)$ for a system of size 1024×1024. The distribution $N(s,L)$ exhibits a power law with a slope of 1.93 ± 0.05. In the inset, a data collapse of different system sizes is shown with a size dependency of $\chi = 1.8$. The lower figure shows the cumulative distribution $N(s' > s, L)$ for different system sizes $L \times L$ going from $L = 256$ to $L = 1024$. The distributions have slopes around 0.91 ± 0.03. This combined with the data in the upper figure indicates a value of the critical exponent $\tau = 1.92 \pm 0.04$.

to extract information of critical saturation and critical exponents.

Since the data we analyze are divided into discrete histogram bins we substitute the integral of Eq. (25) with a sum and get for the singular part

$$M_{k,\mathrm{sing}} = \sum_s s^k n_s \propto L^{\chi-2} c^{\tau-1-k}, \tag{26}$$

with the assumption that $\chi - 2 < 0$, where χ was defined in Eq. (10).

The total kth moment is [17]

$$M_k = A_k + B_k c + C_k c^{\tau-1-k}, \tag{27}$$

where the last term stems from the singular part and dominates for $k \geq 2$, since the finite-size contribution from Eq. (26) is small.

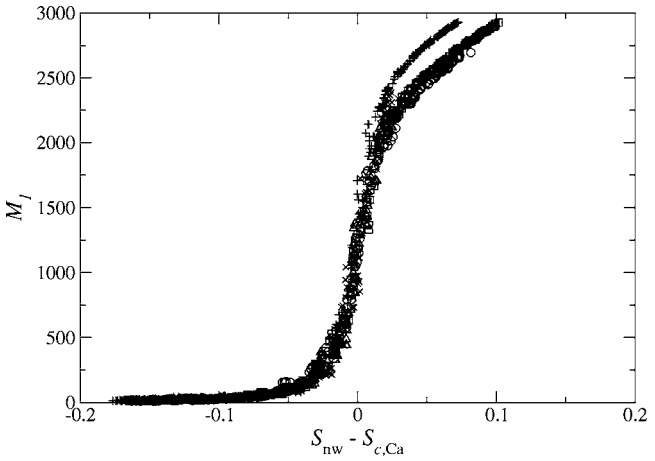

FIG. 8. First moment of the largest cluster plotted as a function of saturations S_{nw} for $L=512$. The three curves are hence for $Ca=3.2\times10^{-3}$, $Ca=3.2\times10^{-4}$, and $Ca=3.2\times10^{-5}$. The percolation thresholds are shifted towards higher values of S_{nw} as Ca increases. The transitions are located at approximately $S_c=0.675$, $S_c=0.7$, and $S_c=0.725$ and hence collapsed.

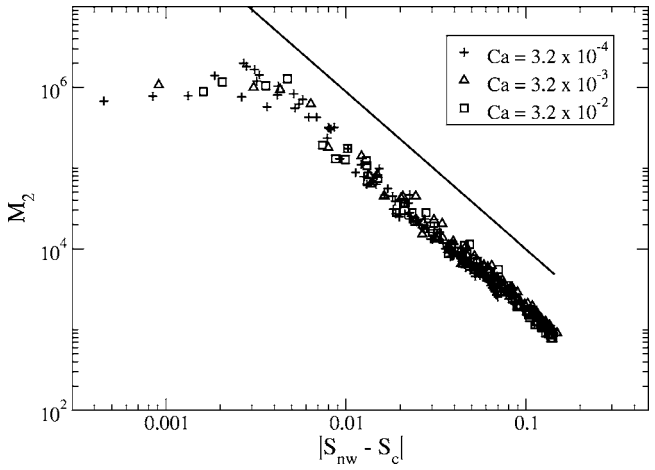

FIG. 9. Log-log plot of the second moment for different Ca for $L=512$. The data are collapsed using the values for S_c obtained previously. There is only a narrow range where the power law is valid due to finite-size effects. For $S_{nw}<S_c$ far away from S_c we see a cutoff and for $|S_{nw}-S_c|\ll 1/L^{1/\nu}$ the function approaches a constant. However, the obtained value $\tilde{\gamma}=1.95\pm0.06$ is reasonable.

In particular, the second moment M_2 is dominated by $M_{2,\mathrm{sing}}$ and

$$M_2 \propto M_{2,\mathrm{sing}} = C_2 L^{\chi-2} c^{\tau-3} \propto |S-S_c|^{-(3-\tau/\sigma)-(\chi-2)\nu} = |S-S_c|^{-\tilde{\gamma}}, \tag{28}$$

when $s^* \sim L^D$ near critical saturation. Then $(\chi-2)\nu$ gives a correction to the exponent $\gamma=(3-\tau)/\sigma$ from ordinary percolation theory, and $\tilde{\gamma}=\gamma+(\chi-2)\nu$.

Results from different calculations of M_2 for different values of Ca are shown in Fig. 8. We notice that there are two regimes in the plot separated by a crossover at a certain value of $|S_{nw}-S_c|$.

This can be understood as finite-size scaling, where near a critical density p_c we apply the finite-size ansatz

$$\Pi = \Phi[(p-p_c)L^{1/\nu}]. \tag{29}$$

This implies that the effective, critical density p_{eff} is

$$p_{\mathrm{eff}} = \int p\left(\frac{d\Pi}{dp}\right)dp. \tag{30}$$

Hence, in our case we use this expression with our saturation for the variable p and get

$$S_{\mathrm{eff}} = S_c + \frac{A}{L^{1/\nu}}. \tag{31}$$

Setting this new critical saturation in for S_c in Eq. (28) we see the two regimes as

$$M_2 \propto |S_{nw}-S_c|^{\tilde{\gamma}} \quad \text{for } |S_{nw}-S_c| \gg \frac{A}{L^{1/\nu}},$$

$$M_2 \propto \text{const} \quad \text{for } |S_{nw}-S_c| \ll \frac{A}{L^{1/\nu}}, \tag{32}$$

when only S_{nw} varies and L is constant.

The critical saturations are moving towards larger values as Ca increases. Since the fluctuations around the critical saturations are large, it is difficult to establish accurate value of S_c. However, Fig. 9, with the different values of S_{eff} obtained in Fig. 8, gives a power-law behavior with $\tilde{\gamma}=1.95\pm0.06$. This value is significantly lower than the percolation value of γ but this can be understood partly from the system size correction $\chi-2\neq0$.

Since the critical value of saturation of nonwetting fluid decreases with the capillary number, we expect more or less an approach towards percolation for extremely low Ca. On the other hand, when viscous forces are totally dominant and $Ca\to\infty$, the expected threshold should be around unity. This expectation is based on the presumption that tiny bubbles of

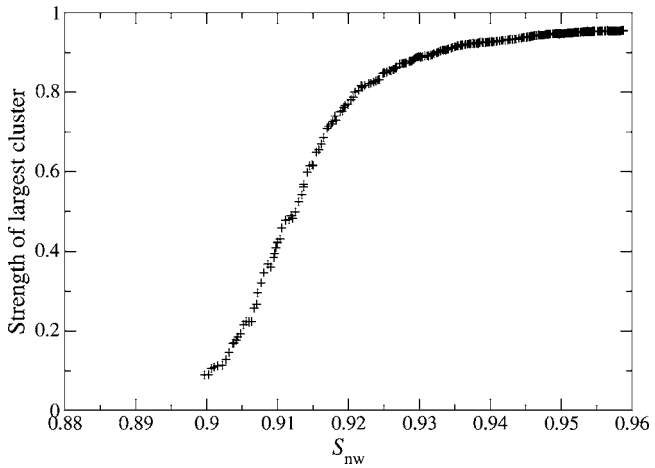

FIG. 10. Strength of largest nonwetting cluster for $Ca\to\infty$. The data indicate a threshold at $S_{nw}=0.91$ which is lower than unity. We can explain this by a lower cutoff of small clusters which will be of significance when operating with no surface tension. The data are from system size $L=512$ and taken from the mean of ten different runs.

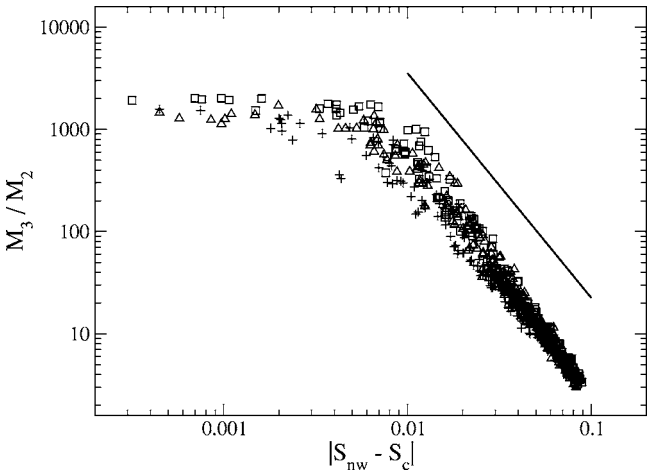

FIG. 11. Log-log plot of the ratio M_3/M_2 for $L=512$. The solid line has a slope of -2.14 and gives $1/\sigma=2.14\pm0.08$ using Eq. (33). This gives $\sigma=0.47\pm0.08$.

either phase will be overrepresented and effectively break up large clusters forming out of one fluid phase. Then no spanning nonwetting cluster can form, even at very high S_{nw}.

It is of course a matter of view how small we accept such bubbles to be, because at some point we must regard nodes to be connected even though microscopic fragments of wetting fluid separate them. These microscopic clusters, which we disregard in our calculations, do have an effect on S_c as can be seen in Fig. 10. Here we see $S_c=0.91$ which is significantly lower than unity.

In order to find a value for σ, we use the ratio

$$\frac{M_{k+1}}{M_k} = \frac{1}{c}, \quad \text{for } k \geqslant 2. \tag{33}$$

Then we can easily find an estimate for σ, and even though there is a finite-size correction to the scaling of M_k, this will vanish when we measure the ratio in Eq. (33).

The measured value of σ from the relation $c \propto |S_{\mathrm{nw}} - S_c|^{1/\sigma}$ is shown in Fig. 11. We find $\sigma=0.47\pm0.08$, but this value is dependent of the chosen value of the critical saturation S_c. This value is arguable. However, the ratio of $\tilde{\gamma}$ and σ is assumed to be constant, and hence the value of τ in our simulations. Since $D=1/\sigma\nu$ we get the relation

$$\tilde{\gamma}\sigma = 3 - \tau + \frac{\chi - 2}{D}. \tag{34}$$

There are of course uncertainties connected to the size effects related to $\chi-2$, but with the data collapse in Fig. 7 which suggested a $\chi-2=-0.2$ and a fractal dimension for the nonwetting clusters in the area $D=1.82-1.89$ [21,27], the relation above should give a $\tau\approx1.97$. This is consistent with our measured $\tau=1.92\pm0.04$.

V. CONCLUSION

In this paper we have presented results of cluster distribution in a two-phase flow network simulator in two dimensions. Different from most studies of porous flow simulations in networks, we apply *biperiodic boundary conditions*. This allows us to study steady-state conditions which are more similar to those encountered deep inside natural reservoirs.

The simulations show that there is a crossover from unstable front propagation to a compact steady-state flow as the patterns formed by initial transients are broken up. From the pressure development in Fig. 3 this change in flow regime will result in an increase in ΔP and a more violent evolution of burst avalanches. We believe that the fragments of nonwetting fluid sustain their fractal properties, but the S_{nw} at which we get spanning nonwetting clusters is dependent on *Ca* even though the fractal front is completely dissolved.

The steady-state distribution of clusters is shown to share many characteristics with that of ordinary percolation when it comes to critical properties and the extraction of critical exponents. We find a power-law distribution of nonwetting clusters near critical saturation. This is obtained regardless of the initial organization of fluids outside the steady-state regime. Even though $\tau=1.92\pm0.04$ is slightly lower than the value for pure percolation it is consistent with results obtained from other dynamical models and fragmentation studies [30]. From the order parameter $P_\infty \propto (S-S_c)^\beta$, nonnegativity of the exponent $\beta>0$ may be ensured even though $\tau<2$. This is shown through a finite-size analysis.

ACKNOWLEDGEMENT

We thank Martin Ferer, Henning A. Knudsen, and Knut Jørgen Måløy for very helpful discussions. This work has been financed through Norwegian Research Council (NFR) Grant No. 154535/432 and parts of the computations were done on the Norwegian HPC Program NOTUR.

[1] J. D. Chen and D. Wilkinson, Phys. Rev. Lett. **55**, 1892 (1985).
[2] K. J. Måløy, J. Feder, and T. Jøssang, Phys. Rev. Lett. **55**, 2688 (1985).
[3] R. Lenormand, E. Touboul, and C. Zarcone, J. Fluid Mech. **189**, 165 (1988).
[4] J. Koplik and T. J. Lasseter, Soc. Pet. Eng. J. **2**, 89 (1985).
[5] M. Blunt and P. King, Phys. Rev. A **42**, 4780 (1990).
[6] D. Rothman, J. Geophys. Res. **95**, 8663 (1990).
[7] D. Wilkinson and J. F. Williams, J. Phys. A **16**, 3365 (1983).
[8] P. Binning and M. A. Celia, Adv. Water Resour. **22**, 461 (1998), and references therein.
[9] E. Aker, K. J. Måløy, A. Hansen, and G. G. Batrouni, Transp. Porous Media **32**, 163 (1998).
[10] H. A. Knudsen, E. Aker, and A. Hansen, Transp. Porous Media **47**, 99 (2002).
[11] F. A. L. Dullien, *Porous Media: Fluid Transport and Pore Structure*, 2nd ed. (Academic Press, San Diego, 1992).

[12] S. Roux (unpublished).
[13] H. A. Knudsen and A. Hansen, Phys. Rev. E **65**, 056310 (2002).
[14] E. Aker, K. J. Måløy, A. Hansen, and S. Basak, Europhys. Lett. **51**, 55 (2000).
[15] E. Aker, K. J. Måløy, and A. Hansen, Phys. Rev. Lett. **84**, 4589 (2000).
[16] J. Ferkinghoff-Borg, M. H. Jensen, J. Mathiesen, P. Olesen, and K. Sneppen, Phys. Rev. Lett. **91**, 266103 (2003).
[17] M. F. Gyure, M. V. Ferer, B. F. Edwards, and G. Huber, Phys. Rev. E **51**, 2632 (1995).
[18] S. Redner, in *Statistical Models for Fracture of Disordered Media*, edited by H. J. Herrmann and S. Roux (Elsevier Science, Amsterdam, 1990), Chap. 10 and references therein.
[19] R. Lenormand and C. Zarcone, Phys. Rev. Lett. **54**, 2226 (1985).
[20] P. Meakin, Physica A **173**, 305 (1991).
[21] O. I. Frette, K. J. Måløy, J. Schmittbuhl, and A. Hansen, Phys. Rev. E **55**, 2969 (1997).
[22] L. Furuberg, J. Feder, A. Aharony, and T.Jossang, Phys. Rev. Lett. **61**, 2117 (1986).
[23] D. Wilkinson, Phys. Rev. A **34**, 1380 (1986).
[24] M. Ferer, G. S. Bromhal, and D. H. Smith, Phys. Rev. E **71**, 026303 (2005).
[25] D. Stauffer and A. Aharony, *Introduction to Percolation Theory* (Taylor & Francis Ltd., London, 1994).
[26] J. Hoshen and R. Kopelman, Phys. Rev. B **14**, 3438 (1976).
[27] G. Wagner, A. Birovljev, P. Meakin, J. Feder, and T. Jøssang, Phys. Rev. E **55**, 7015 (1997).
[28] T. Vicsek and F. Family, Phys. Rev. Lett. **52**, 1669 (1984).
[29] N. Martys, M. O. Robbins, and M. Cieplak, Phys. Rev. B **44**, 12294 (1991).
[30] F. Kun and H. J. Herrmann, Comput. Methods Appl. Mech. Eng. **138**, 3 (1996).